Single-Ion Conducting Multi-block Copolymer Electrolyte for Lithium-Metal Batteries with High Mass Loading $NCM_{8\,11}$ Cathodes

Xu Dong, Alexander Mayer, Xu Liu, Stefano Passerini,* and Dominic Bresser*

ABSTRACT: Lithium-metal batteries comprising a single-ion conducting polymer electrolyte and a nickel-rich $LiNi_{1-x-y}Co_xMn_yO_2$ (NCM) positive electrode (cathode) potentially offer v ery h igh e nergy d ensity a nd g reat s afety. However, such cell chemistry is very demanding concerning the required interfacial stability of the polymer electrolyte, and the realization of high mass loading cathodes remains a great challenge. Herein, the development of a new single-ion conducting multi-block copolymer electrolyte including trifluoromethyl g roups i n the ionophilic block is reported. After ethylene carbonate (EC) is incorporated into the self-standing and easily processable polymer membranes, high ionic conductivity along with very high limiting current density and suitable anodic stability are obtained. These enable stable cycling of Li||NCM_{811} cells—also at high C rates (up to 5C) and active material mass loadings of the NCM_{811} cathode of >10 mg cm^{-2}, which are both key steps toward the potential commercialization of this class of electrolytes.

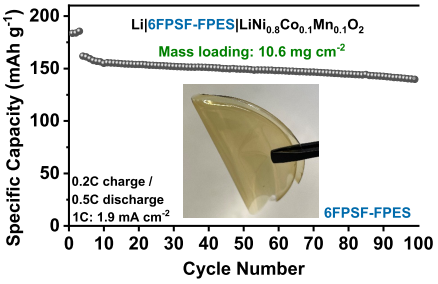

Worldwide concerns about climate change are motivating the development of green energy technologies, including high-performance batteries to allow for the efficient storage of renewable energy.[1−4] To further increase the energy density of lithium batteries, the use of metallic lithium for the negative electrode is considered a key step in the near-term to mid-term future, owing to its high theoretical capacity of 3,860 mAh g^{-1} and very low redox potential of −3.04 V vs the standard hydrogen electrode (SHE).[5−10] The transition from lithium-ion to lithium-metal batteries (LMBs), however, requires the replacement of the commonly used, highly flammable liquid electrolytes (i.e., solutions of $LiPF_6$ in organic carbonates), as they do not form a long-term stable interphase with lithium metal.[11−19]

Polymer electrolytes (PEs) are a potential alternative, offering greater safety combined with a rather easy processability and handling.[20−24] The most investigated class of PEs is poly(ethylene oxide) (PEO) comprising a lithium salt, which was reported first by Wright and co-workers in 1973.[25] Such systems, however, suffer from the mobility of both ionic species—the cation and anion. The latter is frequently more mobile, which results in a relatively low lithium-ion transference number (t_{Li^+}), causing the formation of reversed concentration gradients upon cycling.[26−29] This characteristic, together with the limited ionic conductivity at ambient temperature[20,27,30] and the poor electrochemical stability toward elevated potentials beyond 3.8 V,[31−33] hinders their use in combination with high-voltage cathode materials such as $LiNi_{0.8}Co_{0.1}Mn_{0.1}O_2$ (NCM_{811}). To address these challenges, the design of high-performance single-ion conducting polymer electrolytes (SIPEs)[18,34−42] with the anionic group covalently tethered to the polymer backbone was proposed. This enables a t_{Li^+} close to unity, which helps to suppress dendritic lithium deposition.[35,43−45]

Following our previous findings that revealed a beneficial impact of trifluoromethyl groups on the electrochemical stability in Li||NCM cells,[46] we introduced this moiety in the earlier reported polyarylene-based multi-block copolymer electrolyte (Figure 1a), hereinafter referred to as 6FPSF-FPES.[37,41,47,48] The resulting SIPE provides high ionic conductivity, limiting current density, and electrochemical stability. Moreover, its incorporation in the NCM_{811} electrode enables the realization of high mass loading cathodes, showing stable cycling at reasonable discharge/charge rates for 100 cycles. To the best of our knowledge, this is the highest cathode mass loading reported so far in combination with SIPEs.

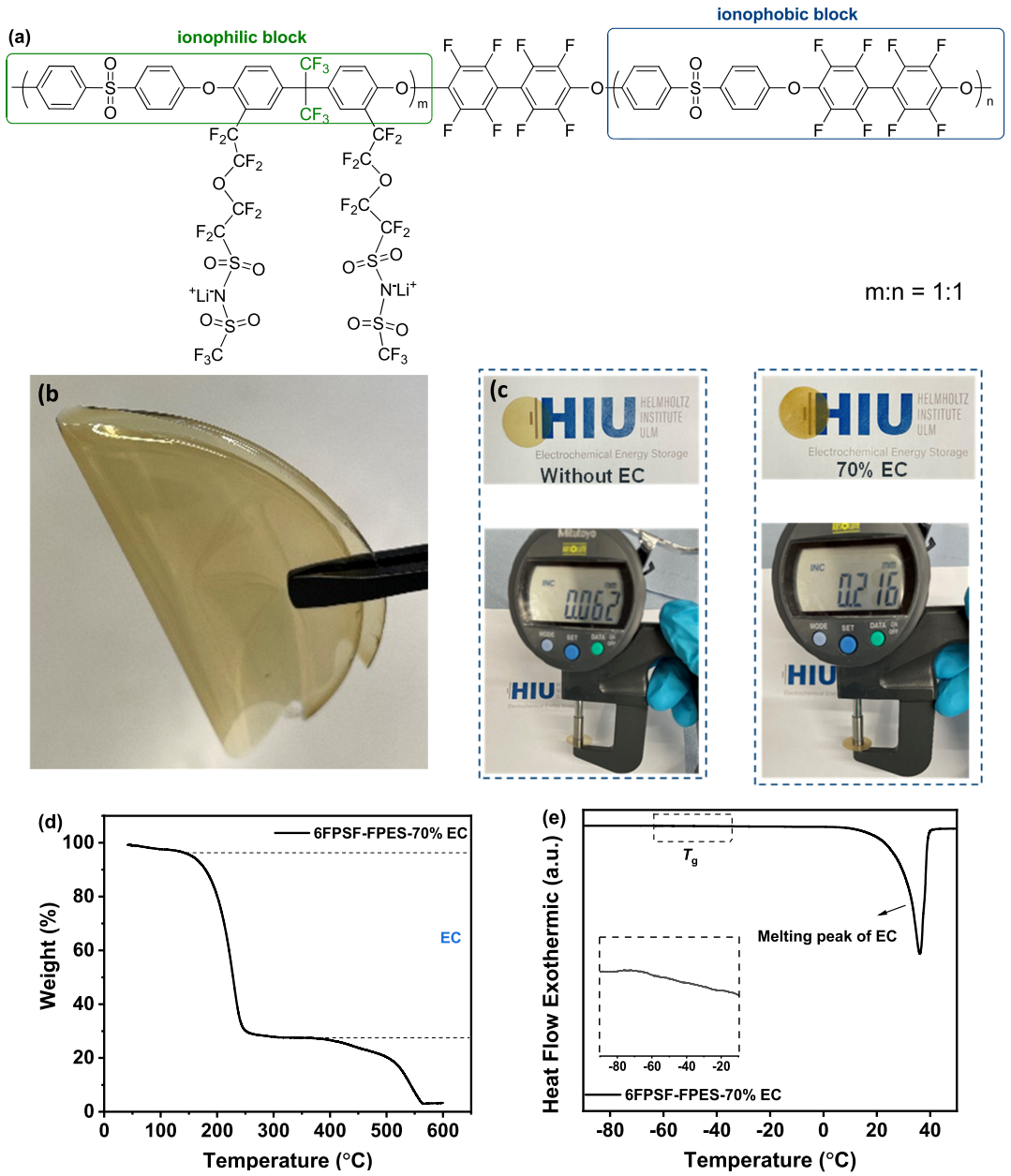

Figure 1. (a) Chemical structure of the 6FPSF-FPES ionomer. (b) Photograph of the 6FPSF-FPES membrane obtained by solvent-casting. (c) Photographs documenting the determination of the thicknesses of the readily punched membranes before and after incorporation of EC. (d) TGA data recorded for 6FPSF-FPES-70% EC. (e) DSC curve recorded for 6FPSF-FPES-70% EC (2nd cycle heating).

The molecular structure of 6FPSF-FPES is given in Figure 1a, with the trifluoromethyl groups in the ionophilic part of the polymer backbone highlighted in green. The synthesis is described in detail in the Supporting Information, along with basic characterization via ^{1}H NMR and ^{19}F NMR spectroscopy (Figures S1–S3), gel permeation chromatography (GPC; Table S1), and FT-IR spectroscopy (Figure S4). Solvent casting of the ionomer yields transparent, self-standing, and flexible membranes (Figure 1b). Subsequently, circular membranes with a diameter of 15 mm were punched and soaked with 70 wt% ethylene carbonate (EC), which results in a significant increase in thickness from about 62 to 216 μm (Figure 1c). The thermal stability of these soaked membranes was evaluated by thermogravimetric analysis (TGA; Figure 1d). The mass loss from 150 to 250 °C is attributed to the evaporation of EC (see also Figure S5 for the TGA of EC only for comparison). The ionomer itself is stable until about 350 °C, which makes it very suitable for practical application in LMBs. The differential scanning calorimetry (DSC) plot (Figure 1e) exhibits a sharp endothermic peak (onset temperature: 29.8 °C; peak temperature: 36.1 °C) due to the melting of EC and a glass transition at around −26.3 °C, which is in very good agreement with previous findings for the ionophilic block.[37] The mechanical properties of the EC-containing ionomer beyond the melting point of EC are qualitatively displayed in Video S1.

The electrochemical properties of the 70 wt% EC-containing ionomer membranes were also investigated (Figure 2). The temperature-dependent ionic conductivity is shown in Figure 2a. At 30 °C the ionic conductivity is relatively low, but it substantially increases at 40 °C and beyond owing to the melting of EC between these two temperatures. In fact, at 40

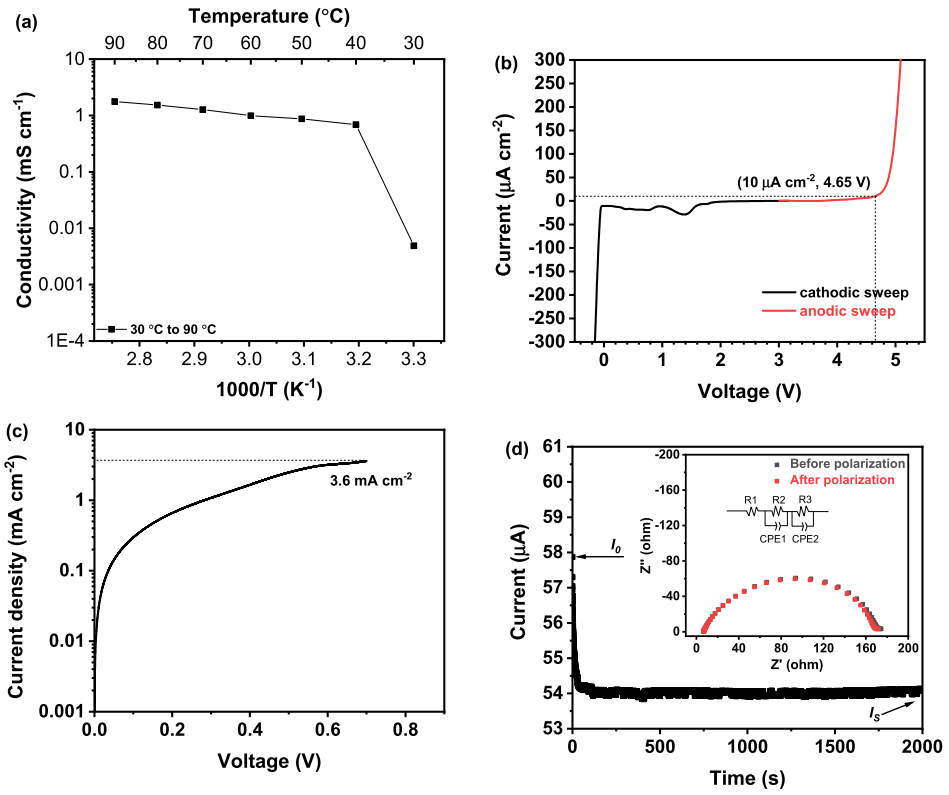

Figure 2. (a) Ionic conductivity of 6FPSF-FPES-70% EC as a function of temperature. Determination of (b) the electrochemical stability via LSV (Li||Ni cells; sweep rate: 1.0 mV s^{-1}; 40 °C) and (c) the limiting current density (Li||Li cells; sweep rate: 0.02 mV s^{-1}; 40 °C). (d) Plot of the resulting current after a voltage of 10 mV is applied to the cell, with an indication of the current values used for the calculation of the Li^+ transference number; as inset the corresponding Nyquist plots for the EIS measurements before and after polarization are shown.

°C the conductivity is as high as 0.69 mS cm^{-1} (see Table S2 and Figure S6 for a comparison of the ionic conductivity at 40 °C with varying EC content), and at 90 °C it significantly exceeds 1 mS cm^{-1}, at 1.77 mS cm^{-1}. At 40 °C the ionic conductivity is almost twice the value (0.4 mS cm^{-1}) required for electric vehicle applications.[49] Also the electrochemical stability appears to be very suitable, at about 4.65 V toward oxidation at 40 °C (current threshold: 10 μA cm^{-2}) and the characteristic minor decomposition traces of EC and potentially DMSO traces upon reduction.[37,50] A truly remarkable value, though, was found for the limiting current density, which was determined to be as high as 3.6 mA cm^{-2} (Figure 2c). This is much higher than the values obtained earlier for similar SIPEs at 40 °C (i.e., about 1.2 mA cm^{-2},[37] and 1.57 mA cm^{-2}),[41] indicating that the introduction of the trifluoromethyl groups has a beneficial impact on the electrochemical properties beyond the interfacial stability.[46] Completing the basic electrochemical characterization, the lithium transference number (t_{Li}^+) was determined following the method reported by Evans, Vincent, and Bruce.[51] The corresponding chronoamperometry (CA) and electrochemical impedance spectroscopy (EIS) data are presented in Figure 2d, including also the equivalent model circuit used for analysis of the EIS data. The current initially drops very rapidly after the voltage excitation and then reaches a steady state. The electrolyte resistance remains the same before and after the polarization (i.e., after having reached the steady state), at about 6.7 Ω cm^{-2}. The interfacial resistance decreases slightly from 165.2 Ω cm^{-2} to 161.3 Ω cm^{-2}, which might be related to a minor reorganization of the ionic groups at the electrodel electrolyte interface, benefiting the charge transfer across the interface. Using eq S2, the cationic transference number was calculated to be 0.93, which is fairly close to unity and, thus, corroborates the expected single-ion conducting behavior.

The dynamic stability of the lithium|electrolyte interface was further investigated by conducting lithium stripping and plating experiments in symmetric Li||Li cells at 40 °C. The cells were subjected to an alternating and varying current density for 1 h each, ranging from ±5 to ±500 μA cm^{-2} (Figure 3a). With increasing current density, the overpotential increases essentially linearly (i.e., doubling the current density results in a 2-fold overpotential increase) but remains constant. However, a slight increase upon cycling is observed for the highest current density (500 μA cm^{-2}). Figure 3b displays the magnification of a few selected cycles at each current density, indicated by the dashed frames in Figure 3a. For all current densities up to 300 μA cm^{-2}, the cycling profiles reveal the constant voltage response expected for single-ion conducting electrolyte systems. At the maximum current density of 500 μA cm^{-2}, however, the voltage response shows a slight increase upon stripping and plating. This observation indicates that the maximum current density that can be applied to the system is limited to less than 500 μA cm^{-2}, while higher current densities are limited to discharge/charge pulses. Nonetheless, the subsequent evaluation of the long-term stripping/plating behavior at 50 μA cm^{-2} revealed an excellent reversibility and an essentially constant overpotential of about 12 mV for more than 1,600 h (Figure 3c), indicating a very good interfacial stability of the 6FPSF-FPES electrolyte system.

Motivated by these very good electrochemical properties of the 6FPSF-FPES ionomer, we assembled Li||NCM_{811} cells to investigate the performance in combination with state-of-the-

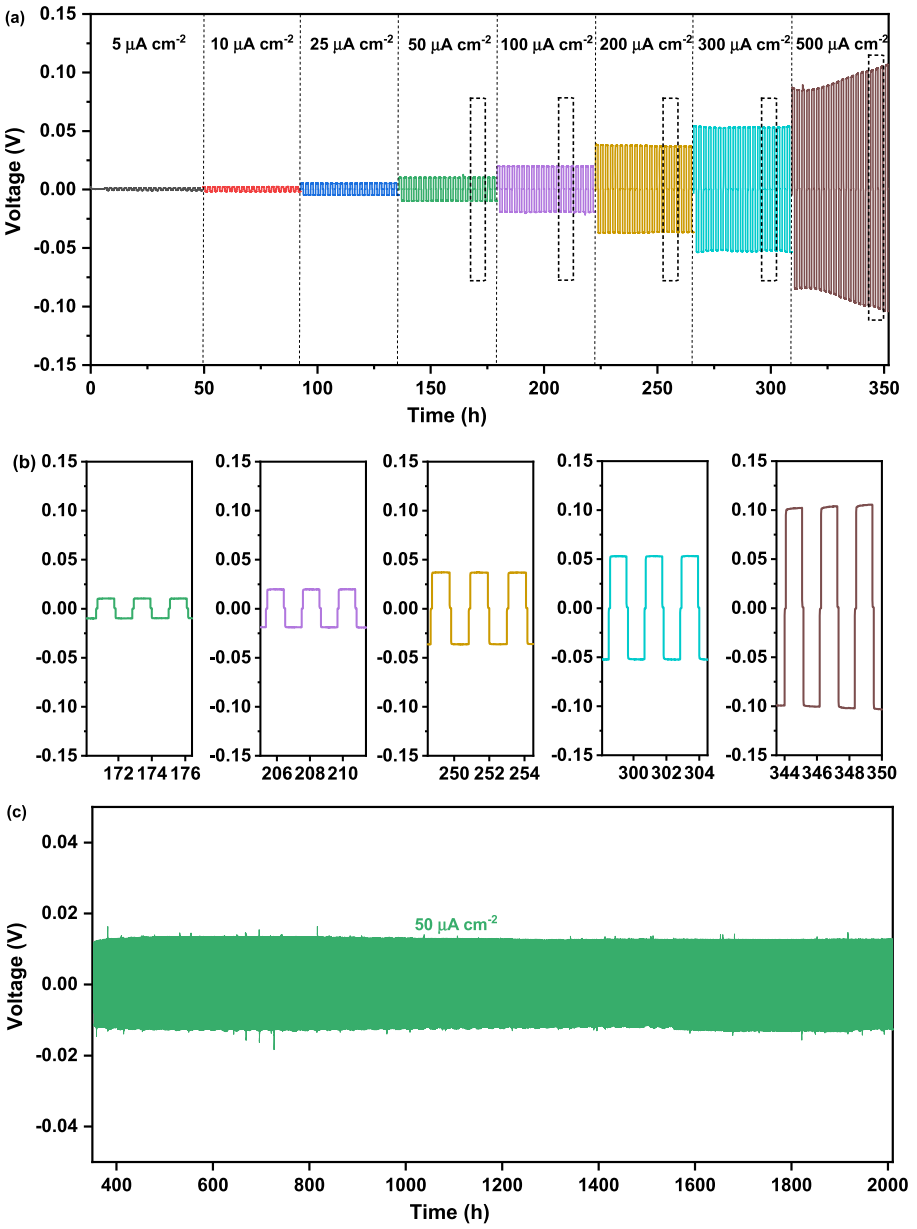

Figure 3. (a) **Voltage profiles of Li|6FPSF-FPES-70% EC|Li cells at various current densities (40 °C). (b) Magnification of exemplary voltage profiles at different current densities. (c) Galvanostatic lithium stripping and plating at a constant current density of 50 μA cm^{-2}, conducted in Li||Li cells (40 °C).**

art high-energy cathode materials (Figure 4). Figure 4a,b shows the rate capability and the corresponding discharge/charge profiles when the cut-off voltages were set to 3.0 and 4.2 V. The cells demonstrate a high reversible (discharge) capacity of 180 mAh g^{-1} at 0.1C, which slightly decreases to ca. 160, 150, 140, 125, and 115 mAh g^{-1} at 0.3C, 0.5C, 1C, 2C, and 3C, respectively, owing to the stepwise increase in polarization (Figure 4b). Remarkably, the cell still shows a relatively high reversible capacity of 94 mAh g^{-1} at 5 C. When the discharge/charge rate was lowered to 0.3C again after the cycling at 5C, the capacity increased back to the same value as before, i.e., ca. 160 mAh g^{-1}. This very good rate capability is assigned to the high ionic conductivity, a suitable interfacial contact, and the high limiting current density. Subsequently, the long-term cycling stability of such Li||NCM$_{811}$ cells was evaluated at 0.2C (Figure 4c,d), 1C (Figure 4e,f), and 2C (Figure 4g,h). Generally, the cells show stable cycling at all discharge/charge rates, though the capacity retention increases from lower to higher rates, i.e., from 83.6% at 0.2C and 95.0% at 1C after more than 160 cycles, to 84.5% after more than 300 cycles at 2C (equivalent to a current density of 0.874 mA cm^{-2}). This trend is also reflected in the average Coulombic efficiency increasing from 99.6% at 0.2C to 99.7% at 2C—presumably owing to the relatively shorter time at elevated potentials when increasing the discharge/charge rate—and the relatively greater increase in polarization (compare, for instance, Figure 4d and Figure 4f; note that a minor fluctuation in Coulombic efficiency and specific capacity in Figure 4c,e,g originates from a power shutdown of the cycler and the climatic chambers). Additionally, the rate capability was tested using the 4.3 V upper cut-off to exploit higher capacities upon elevated charge rates (Figure S7) while using lower anodic cut-offs when cycling at relatively low discharge/charge rates to maximize the lifetime of the battery cell. The initial specific capacity at 0.1C

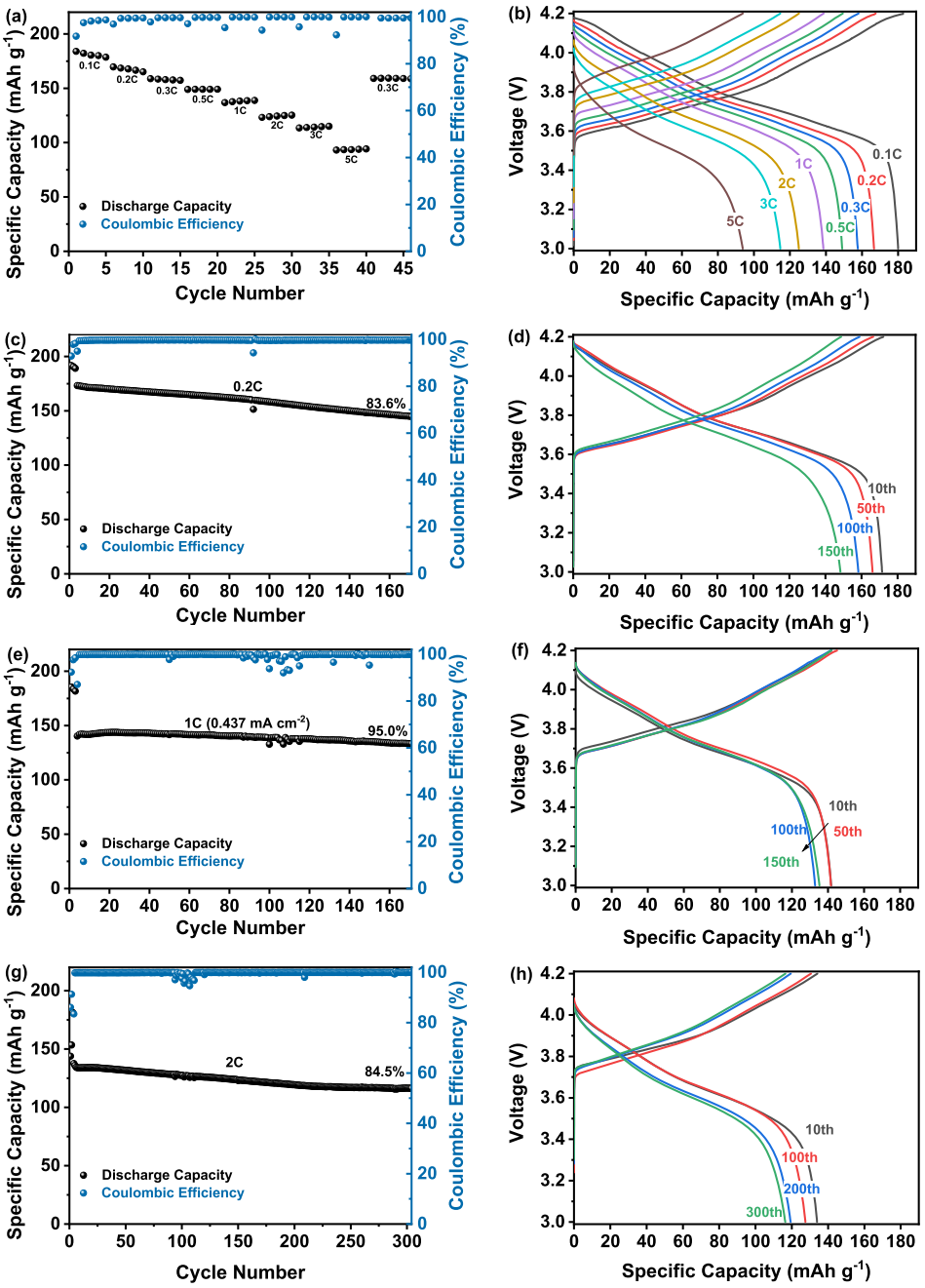

Figure 4. (a) Evaluation of the discharge/charge rate performance of Li||NCM_{811} cells comprising 6FPSF-FPES-70% EC as the electrolyte (cut-off voltages: 3.0 and 4.2 V). (b) Exemplary discharge/charge profiles recorded at the different C rates. (c) Constant current cycling of Li||NCM_{811} cells at 0.2C and (d) selected discharge/charge profiles of the 10th, 50th, 100th, and 150th cycles. (e) Constant current cycling of Li||NCM_{811} cells at 1C and (f) selected discharge/charge profiles of the 10th, 50th, 100th, and 150th cycles. (g) Constant current cycling of Li||NCM_{811} cells at 2C and (h) selected discharge/charge profiles of the 10th, 100th, 200th, and 300th cycles. All measurements were conducted at 40 °C.

was higher than 200 mAh g^{-1} and remained stable across all C rates applied. At 1C and 5C, the specific capacity was 158 and 96 mAh g^{-1}, respectively, i.e., higher than that achieved with the lower anodic cut-off of 4.2 V, while a slight decrease in capacity was observed when the C rate was eventually lowered to 0.3C again. These findings show that higher cut-off voltages can be applied for selected cycles in order to boost the power performance but should remain limited with regard to the long-term cycling stability.

Following these "proof-of-principle experiments" with rather light electrodes (average active material mass loading of ca. 2.3 mg cm^{-2}) to exploit the general compatibility of the polymer electrolyte with such Ni-rich cathode materials, electrodes with "industrial-like" mass loadings (10.6 mg cm^{-2}) were explored. The cycling behavior of these electrodes, which comprise 5 wt % of the 6FPSF-FPES ionomer to ensure sufficient ionic conductivity, in Li|6FPSF-FPES|NCM_{811} cells is presented in Figure 5. The cells show a high specific capacity of 161 mAh g^{-1}, with a capacity retention of 86.1% after 100 cycles and a Coulombic efficiency of 99.8% (Figure 5a). The corresponding discharge/charge profiles (Figure 5b) reveal some increase in polarization upon cycling, which might be in part related to the

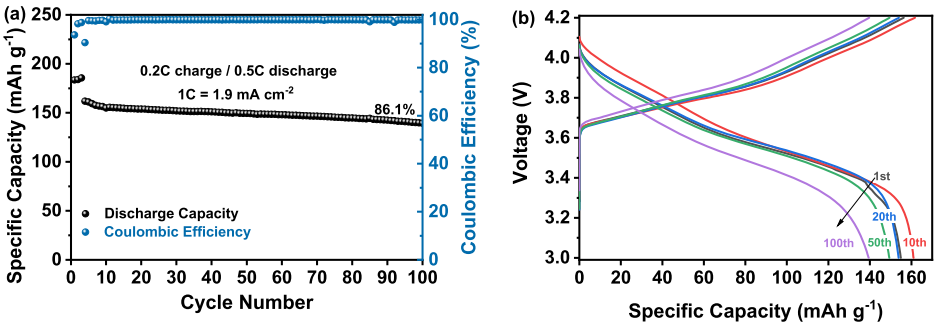

Figure 5. Galvanostatic cycling of Li||NCM_{811} cells comprising NCM_{811} cathodes with a very high active material mass loading of 10.6 ± 0.1 mg cm^{-2} at 40 °C (cut-off voltages: 3.0 and 4.2 V). (a) Plot of the specific capacity as a function of cycle number (first three cycles: 0.05C; subsequently the cell was charged at 0.2C and discharged at 0.5C). (b) Selected discharge/charge profiles of the 1st, 10th, 20th, 50th, and 100th cycles.

need for a further enhanced electrode design and polymer electrolyte incorporation. Nonetheless, the results also show that industrially relevant electrode mass loadings are generally feasible. In fact, to the best of our knowledge, this is the first report on a polymer electrolyte with such high mass loading Ni-rich NCM electrodes (see also Table S3 for a comparison with previous studies on related systems).

In summary, a novel multi-block copolymer SIPE has been successfully synthesized. This SIPE is characterized by a high ionic conductivity of 0.69 mS cm^{-1} at 40 °C, a suitable electrochemical stability toward oxidation and metallic lithium, as proven by more than 1,600 h of lithium stripping and plating without a significant increase in overpotential, and a very high limiting current density when 70 wt% of EC was incorporated. Li||NCM_{811} cells comprising this SIPE show stable cycling at varying discharge/charge rates with, for instance, 84.5% capacity retention after more than 300 cycles at 2C. Remarkably, electrodes with an active material mass loading of 10.6 mg cm^{-2} show very good cycling performance for 100 cycles, achieving great average Coulombic efficiency (99.8%) and capacity retention of 86.1%. All in all, these results support a great step forward toward the potential commercialization of SIPEs in lithium batteries.

AUTHOR INFORMATION

Corresponding Authors

Stefano Passerini − *Helmholtz Institute Ulm (HIU), 89081 Ulm, Germany; Karlsruhe Institute of Technology (KIT), 76021 Karlsruhe, Germany;* orcid.org/0000-0002-6606-5304; Email: stefano.passerini@kit.edu

Dominic Bresser − *Helmholtz Institute Ulm (HIU), 89081 Ulm, Germany; Karlsruhe Institute of Technology (KIT), 76021 Karlsruhe, Germany;* orcid.org/0000-0001-6429-6048; Email: dominic.bresser@kit.edu

Authors

Xu Dong − *Helmholtz Institute Ulm (HIU), 89081 Ulm, Germany; Karlsruhe Institute of Technology (KIT), 76021 Karlsruhe, Germany*

Alexander Mayer − *Helmholtz Institute Ulm (HIU), 89081 Ulm, Germany; Karlsruhe Institute of Technology (KIT), 76021 Karlsruhe, Germany*

Xu Liu − *Helmholtz Institute Ulm (HIU), 89081 Ulm, Germany; Karlsruhe Institute of Technology (KIT), 76021 Karlsruhe, Germany;* orcid.org/0000-0003-0532-316X

Notes

The authors declare no competing financial interest.

ACKNOWLEDGMENTS

The authors would like to acknowledge financial support by the Federal Ministry of Education and Research (BMBF) within the FestBatt project (03XP0175B) and the FB2-Poly project (03XP0429B), as well as the financial support by the Helmholtz Association.

REFERENCES

(1) Borah, R.; Hughson, F.; Johnston, J.; Nann, T. On battery materials and methods. *Mater. Today Adv.* **2020**, *6*, 100046.

(2) He, X.; Bresser, D.; Passerini, S.; Baakes, F.; Krewer, U.; Lopez, J.; Mallia, C. T.; Shao-Horn, Y.; Cekic-Laskovic, I.; Wiemers-Meyer, S.; et al. The passivity of lithium electrodes in liquid electrolytes for secondary batteries. *Nat. Rev. Mater.* **2021**, *6*, 1036−1052.

(3) Palacin, M. R. Recent advances in rechargeable battery Mater.: a chemist's perspective. *Chem. Soc. Rev.* **2009**, *38*, 2565−2575.

(4) Bresser, D.; Moretti, A.; Varzi, A.; Passerini, S. The role of batteries for the successful transition to renewable energy sources. *Encyclopedia of Electrochemistry: Online* **2020**, DOI: 10.1002/9783527610426.bard110024.

(5) Armand, M.; Tarascon, J.-M. Building better batteries. *Nature* **2008**, *451*, 652−657.

(6) Liang, X.; Pang, Q.; Kochetkov, I. R.; Sempere, M. S.; Huang, H.; Sun, X.; Nazar, L. F. A facile surface chemistry route to a stabilized lithium metal anode. *Nature Energy* **2017**, *2*, 17119.

(7) Bresser, D.; Hosoi, K.; Howell, D.; Li, H.; Zeisel, H.; Amine, K.; Passerini, S. Perspectives of automotive battery R&D in China, Germany, Japan, and the USA. *J. Power Sources* **2018**, *382*, 176−178.

(8) Zhang, Y.; Zuo, T.-T.; Popovic, J.; Lim, K.; Yin, Y.-X.; Maier, J.; Guo, Y.-G. Towards better Li metal anodes: challenges and strategies. *Mater. Today* **2020**, *33*, 56−74.
(9) Mayer, A.; Steinle, D.; Passerini, S.; Bresser, D. Block copolymers as (single-ion conducting) lithium battery electrolytes. *Nanotechnology* **2022**, *33*, 062002.
(10) Scrosati, B.; Hassoun, J.; Sun, Y.-K. Lithium-ion batteries. A look into the future. *Energy Environ. Sci.* **2011**, *4*, 3287−3295.
(11) Gnanaraj, J.; Zinigrad, E.; Asraf, L.; Gottlieb, H.; Sprecher, M.; Schmidt, M.; Geissler, W.; Aurbach, D. A detailed investigation of the thermal reactions of $LiPF_6$ solution in organic carbonates using ARC and DSC. *J. Electrochem. Soc.* **2003**, *150*, A1533.
(12) Xu, K. Nonaqueous liquid electrolytes for lithium-based rechargeable batteries. *Chem. Rev.* **2004**, *104*, 4303−4418.
(13) Xu, W.; Chen, X.; Ding, F.; Xiao, J.; Wang, D.; Pan, A.; Zheng, J.; Li, X. S.; Padmaperuma, A. B.; Zhang, J.-G. Reinvestigation on the state-of-the-art nonaqueous carbonate electrolytes for 5 V Li-ion battery applications. *J. Power Sources* **2012**, *213*, 304−316.
(14) Zhang, W.-J. A review of the electrochemical performance of alloy anodes for lithium-ion batteries. *J. Power Sources* **2011**, *196*, 13−24.
(15) Ue, M.; Uosaki, K. Recent progress in liquid electrolytes for lithium metal batteries. *Curr. Opin. Electrochem.* **2019**, *17*, 106−113.
(16) Varzi, A.; Raccichini, R.; Passerini, S.; Scrosati, B. Challenges and prospects of the role of solid electrolytes in the revitalization of lithium metal batteries. *J. Mater. Chem. A* **2016**, *4*, 17251−17259.
(17) Lin, D.; Liu, Y.; Cui, Y. Reviving the lithium metal anode for high-energy batteries. *Nat. Nanotechnol.* **2017**, *12*, 194−206.
(18) Kalhoff, J.; Eshetu, G. G.; Bresser, D.; Passerini, S. Safer electrolytes for lithium-ion batteries: state of the art and perspectives. *ChemSusChem* **2015**, *8*, 2154−2175.
(19) Hammami, A.; Raymond, N.; Armand, M. Runaway risk of forming toxic compounds. *Nature* **2003**, *424*, 635−636.
(20) Bresser, D.; Lyonnard, S.; Iojoiu, C.; Picard, L.; Passerini, S. Decoupling segmental relaxation and ionic conductivity for lithium-ion polymer electrolytes. *Mol. Syst. Des. Eng.* **2019**, *4*, 779−792.
(21) Ngai, K. S.; Ramesh, S.; Ramesh, K.; Juan, J. C. A review of polymer electrolytes: fundamental, approaches and applications. *Ionics* **2016**, *22*, 1259−1279.
(22) Wang, G.; He, P.; Fan, L. Z. Asymmetric Polymer Electrolyte Constructed by Metal−Organic Framework for Solid-State, Dendrite-Free Lithium Metal Battery. *Adv. Funct. Mater.* **2021**, *31*, 2007198.
(23) Wright, P. V. Polymer electrolytes—the early days. *Electrochim. Acta* **1998**, *43*, 1137−1143.
(24) Guan, X.; Wu, Q.; Zhang, X.; Guo, X.; Li, C.; Xu, J. In-situ crosslinked single ion gel polymer electrolyte with superior performances for lithium metal batteries. *Chem. Eng. J.* **2020**, *382*, 122935.
(25) Fenton, D.E.; Parker, J.M.; Wright, P.V. Complexes of alkali metal ions with poly (ethylene oxide). *Polymer* **1973**, *14*, 589.
(26) Stephan, A. M.; Nahm, K. Review on composite polymer electrolytes for lithium batteries. *Polymer* **2006**, *47*, 5952−5964.
(27) Zhou, D.; Shanmukaraj, D.; Tkacheva, A.; Armand, M.; Wang, G. Polymer electrolytes for lithium-based batteries: advances and prospects. *Chem* **2019**, *5*, 2326−2352.
(28) Doyle, M.; Fuller, T. F.; Newman, J. The importance of the lithium ion transference number in lithium/polymer cells. *Electrochim. Acta* **1994**, *39*, 2073−2081.
(29) Dees, D. W.; Battaglia, V. S.; Bélanger, A. Electrochemical modeling of lithium polymer batteries. *J. Power Sources* **2002**, *110*, 310−320.
(30) Gauthier, M.; Belanger, A.; Bouchard, P.; Kapfer, B.; Ricard, S.; Vassort, G.; Armand, M.; Sanchez, J.; Krause, L. Large lithium polymer battery development The immobile solvent concept. *J. Power Sources* **1995**, *54*, 163−169.
(31) Xia, Y.; Fujieda, T.; Tatsumi, K.; Prosini, P. P.; Sakai, T. Thermal and electrochemical stability of cathode materials in solid polymer electrolyte. *J. Power Sources* **2001**, *92*, 234−243.
(32) Wang, C.; Wang, T.; Wang, L.; Hu, Z.; Cui, Z.; Li, J.; Dong, S.; Zhou, X.; Cui, G. Differentiated lithium salt design for multilayered PEO electrolyte enables a high-voltage solid-state lithium metal battery. *Adv. Sci.* **2019**, *6*, 1901036.
(33) Zhou, W.; Wang, Z.; Pu, Y.; Li, Y.; Xin, S.; Li, X.; Chen, J.; Goodenough, J. B. Double-layer polymer electrolyte for high-voltage all-solid-state rechargeable batteries. *Adv. Mater.* **2019**, *31*, 1805574.
(34) Tikekar, M. D.; Choudhury, S.; Tu, Z.; Archer, L. A. Design principles for electrolytes and interfaces for stable lithium-metal batteries. *Nature Energy* **2016**, *1*, 16114.
(35) Jeong, K.; Park, S.; Lee, S.-Y. Revisiting polymeric single lithium-ion conductors as an organic route for all-solid-state lithium ion and metal batteries. *J. Mater. Chem. A* **2019**, *7*, 1917−1935.
(36) Zhang, H.; Li, C.; Piszcz, M.; Coya, E.; Rojo, T.; Rodriguez-Martinez, L. M.; Armand, M.; Zhou, Z. Single lithium-ion conducting solid polymer electrolytes: advances and perspectives. *Chem. Soc. Rev.* **2017**, *46*, 797−815.
(37) Nguyen, H.-D.; Kim, G.-T.; Shi, J.; Paillard, E.; Judeinstein, P.; Lyonnard, S.; Bresser, D.; Iojoiu, C. Nanostructured multi-block copolymer single-ion conductors for safer high-performance lithium batteries. *Energy Environ. Sci.* **2018**, *11*, 3298−3309.
(38) Strauss, E.; Menkin, S.; Golodnitsky, D. On the way to high-conductivity single lithium-ion conductors. *J. Solid State Electrochem.* **2017**, *21*, 1879−1905.
(39) Hallinan, D. T., Jr; Balsara, N. P. Polymer electrolytes. *Annu. Rev. Mater. Res.* **2013**, *43*, 503−525.
(40) Zhang, J.; Wang, S.; Han, D.; Xiao, M.; Sun, L.; Meng, Y. Lithium (4-styrenesulfonyl)(trifluoromethanesulfonyl) imide based single-ion polymer electrolyte with superior battery performance. *Energy Storage Mater.* **2020**, *24*, 579−587.
(41) Chen, Z.; Steinle, D.; Nguyen, H.-D.; Kim, J.-K.; Mayer, A.; Shi, J.; Paillard, E.; Iojoiu, C.; Passerini, S.; Bresser, D. High-energy lithium batteries based on single-ion conducting polymer electrolytes and Li [Ni0. 8Co0. 1Mn0. 1] O2 cathodes. *Nano Energy* **2020**, *77*, 105129.
(42) Liang, H. P.; Zarrabeitia, M.; Chen, Z.; Jovanovic, S.; Merz, S.; Granwehr, J.; Passerini, S.; Bresser, D. Polysiloxane-Based Single-Ion Conducting Polymer Blend Electrolyte Comprising Small-Molecule Organic Carbonates for High-Energy and High-Power Lithium-Metal Batteries. *Adv. Energy Mater.* **2022**, *12*, 2200013.
(43) Zhu, Y.; Wang, X.; Hou, Y.; Gao, X.; Liu, L.; Wu, Y.; Shimizu, M. A new single-ion polymer electrolyte based on polyvinyl alcohol for lithium ion batteries. *Electrochim. Acta* **2013**, *87*, 113−118.
(44) Brissot, C.; Rosso, M.; Chazalviel, J.-N.; Lascaud, S. Dendritic growth mechanisms in lithium/polymer cells. *J. Power Sources* **1999**, *81*, 925−929.
(45) Tikekar, M. D.; Archer, L. A.; Koch, D. L. Stability analysis of electrodeposition across a structured electrolyte with immobilized anions. *J. Electrochem. Soc.* **2014**, *161*, A847.
(46) Dong, X.; Chen, Z.; Gao, X.; Mayer, A.; Liang, H.-P.; Passerini, S.; Bresser, D. Single-ion conducting polymer electrolyte with fluorinated backbone and high-concentration ionic group for high-performance lithium-metal batteries. *J. Energy Chem.* **2023**, in press.
(47) Mayer, A.; Ates, T.; Varzi, A.; Passerini, S.; Bresser, D. Novel sulfur-doped single-ion conducting multi-block copolymer electrolyte. *Front. Chem.* **2022**, *10*, 974202.
(48) Steinle, D.; Chen, Z.; Nguyen, H.-D.; Kuenzel, M.; Iojoiu, C.; Passerini, S.; Bresser, D. Single-ion conducting polymer electrolyte for Li‖ LiNi0.6Mn0.2Co0.2O2 batteries—impact of the anodic cutoff voltage and ambient temperature. *J. Solid State Electrochem.* **2022**, *26*, 97−102.
(49) Kim, H.-K.; Srinivasan, V. Status and Targets for Polymer-Based Solid-State Batteries for Electric Vehicle Applications. *J. Electrochem. Soc.* **2020**, *167*, 130520.
(50) Mayer, A.; Nguyen, H.-D.; Mariani, A.; Diemant, T.; Lyonnard, S.; Iojoiu, C.; Passerini, S.; Bresser, D. Influence of Polymer Backbone Fluorination on the Electrochemical Behavior of Single-Ion Conducting Multiblock Copolymer Electrolytes. *ACS Macro Lett.* **2022**, *11*, 982−990.

(51) Evans, J.; Vincent, C. A.; Bruce, P. G. Electrochemical measurement of transference numbers in polymer electrolytes. *Polymer* **1987**, *28*, 2324−2328.